

Statistical analysis of landslides caused by the Mw 6.9 Yushu, China, earthquake of April 14, 2010

Chong Xu · Xiwei Xu

Received: 3 June 2013 / Accepted: 7 January 2014 / Published online: 17 January 2014
© Springer Science+Business Media Dordrecht 2014

Abstract The April 14, 2010 Yushu, China, earthquake (Mw 6.9) triggered a great number of landslides. At least 2,036 co-seismic landslides, with a total coverage area of 1.194 km², were delineated by visual interpretation of aerial photographs and satellite images taken following the earthquake, and verified by field inspection. Based on the mapping results, a statistical analysis of the spatial distribution of these landslides is performed using the landslide area percentage (LAP), defined as the percentage of the area affected by the landslides, and landslide number density (LND), defined as the number of landslides per square kilometer. The purpose is to clarify how the landslides correlate the control factors, which are the elevation, slope angle, slope aspect, slope position, distance from drainages, lithology, distance from the surface rupture, and peak ground acceleration (PGA). The results show that both LAP and LND have strongly positive correlations with slope angle and negative correlations with distance from the surface rupture and distance from drainages. The highest LAP and LPD values are in places of elevations from 3,800 to 4,000 m. The slopes producing landslides are mostly facing toward NE, E, and SE. The geological units of *Q_{4al-pl}*, *N*, and *T_{3kn}¹* have the highest concentrations of co-seismic landslides. No apparent correlations are present between LAP and LND values and PGA. On both sides of the surface rupture, the landslide distributions are almost similar except a few exceptions, likely associated with the nature of the strike-slip seismogenic fault for this event. The bivariate statistical analysis shows that, in descending order, the earthquake-triggered landslide impact factors are distance from surface rupture > slope angle > distance from drainages > lithology > PGA. Besides, as the detailed co-seismic landslides inventories related to strike-slip earthquakes are still few compared with that of thrusting-fault earthquakes, this case study would shed new light on the subject. For instance, the

C. Xu (✉) · X. Xu

Key Laboratory of Active Tectonics and Volcano, Institute of Geology, China Earthquake Administration, 1# Huayanli, Chaoyang District, PO Box 9803, Beijing 100029, People's Republic of China

e-mail: xc11111111@126.com; xuchong@ies.ac.cn

X. Xu

e-mail: xiweixu@vip.sina.com

landslide spatial distribution on both sides of the strike-slip seismogenic fault is rather different from that of thrusting-fault earthquakes. It reminds us to take different strategies of measures for prevention and mitigation of landslides induced by earthquakes with different mechanisms.

Keywords 2010 Yushu earthquake · Landslide · Statistical analysis · Landslide area percentage · Landslide number density · Control factor

1 Introduction

At 07:49 (Beijing time) on April 14, 2010, a catastrophic earthquake with Ms 7.1 struck Yushu County in Qinghai Province, China [China Earthquake Networks Center (CENC) www.cenc.ac.cn; Xu et al. 2013a). This earthquake was known as the Yushu earthquake as its epicenter was located in the administrative region of the county (Fig. 1). The USGS reported a moment magnitude (M_w) of 6.9 for this event. Its epicenter was located at latitude 33.2°N , longitude 96.6°E with a focal depth of 14 km according to CENC or latitude 33.224°N , longitude 96.666°E with a focal depth of 17 km according to the USGS. According to the Government of China, as of May 30, 2010 at 18:00, 2,698 people were confirmed dead, 270 missing, and 12,135 injured in this earthquake, and also almost 15,000 houses were destroyed. Inventory compiling and spatial distribution analyses of earthquake-triggered landslides are important in understanding which areas are most susceptible to landsliding in future earthquakes (Harp et al. 2011; Xu et al. 2012a, b). A statistical analysis of 40 historical worldwide earthquake-triggered landslide distributions was performed by Keefer (1984). A database of earthquake-triggered landslides for events from 1980 to 1997, compiled by Rodríguez et al. (1999), extends the work of Keefer (1984). Later, there were many publications focused on inventory compiling of co-seismic landslides triggered by individual earthquake events (Table 1) and general correlations analyzing co-seismic landslides occurrence with topographic and geologic parameters, earthquake conditions related to individual earthquake events. In addition to co-seismic landslide spatial distribution analyses, detailed co-seismic landslide inventories are also essential and important to landslides hazard assessment (Xu et al. 2012a, b, d; Lee et al. 2008), topography evolution of the earthquake areas (Parker et al. 2011), controlling of active fault on landslide spatial distribution patterns (Xu et al. 2013b, c; Gorum et al. 2011), as well as inversion of earthquake-associated features (Xu et al. 2013e; Meunier et al. 2013; Jiang et al. 2013).

The purpose of this paper is to characterize the spatial distribution of the landslides by using a statistical analysis based on the mapping results. It employs two parameters: landslide area percentage (LAP), defined as the percentage of the area affected by landslides, and landslide number density (LND), defined as the number of landslides per square kilometer. We correlate these two parameters with the impact factors that control the earthquake-triggered landslides occurrence. These factors are elevation, slope angle, slope aspect, slope position, distance from drainages, lithology, distance from co-seismic surface rupture, and peak ground acceleration (PGA). They are further grouped into topographic, geological, and earthquake parameters (Table 2). In addition, the influences of morphometric parameters including length, width, and landslide aspect ratios, as well as the nature of the seismogenic fault on landslides are also analyzed.

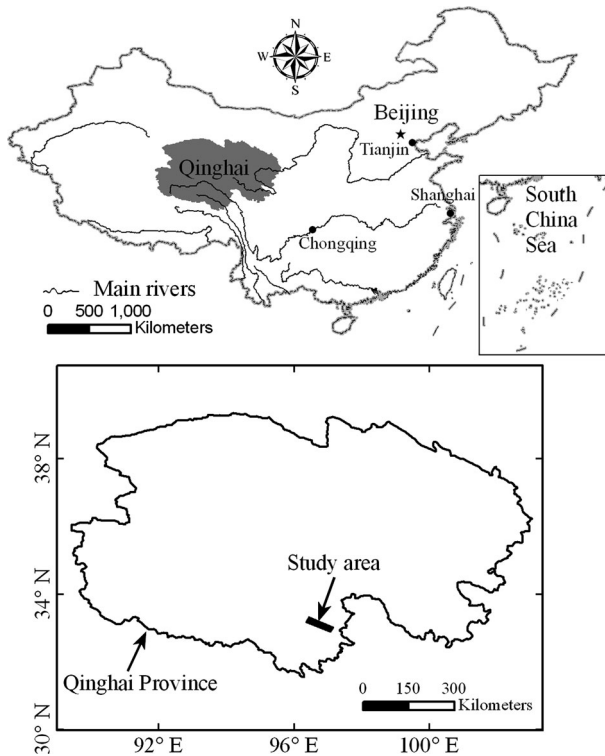


Fig. 1 Location of the study area

2 Tectonic setting

The Yushu earthquake occurred on the Garzê-Yushu fault, a sinistral strike-slip fault on the western segment of the Xianshuihe fault zone; 40 km west of Jiegu Town, Yushu County, Qinghai Province, in the eastern Tibetan Plateau. After the quake, the Jiegu and Jielong towns were severely affected, and a 300°-striking, 65-km-long surface rupture zone was seen along the fault. The surface rupture zone consists of shear, transtensional, transpressional, and tension cracks, as well as mole tracks in right-stepovers and small pull-aparts in left-stepovers between en echelon cracks with left-lateral components (Xu et al. 2010a). The average left-lateral slip is 1 m with a maximum slip of 2.4 m. The surface rupture zone can be divided into two relatively independent sections: the Jielong section and Jiegu section. The former is 15 km long with a maximum left-lateral slip of 0.66 m, while the latter is about 31 km long with a maximum left-lateral slip of 2.4 m, located near the Guoyangyansongduo Village. The two independent sections correspond to a Mw 6.4 sub-event and to a Mw 6.9 sub-event, respectively (Fig. 2). The Mw 6.4 sub-event was initiated on the Jielong sub-fault near the epicenter, which is dominated by left-lateral slip with normal slip component. The other sub-event triggered left-lateral slip on the Jiegu sub-fault to produce the Mw 6.9 sub-event. (Xu et al. 2010a, 2013a; Pan et al. 2010; Wu et al. 2010; Chen et al. 2010).

More than 20 earthquake have been ruptured the surface in the past 100 years along the Garzê-Yushu fault, the Eastern Kunlun fault, and the Longmenshan thrust belt, which

Table 1 Co-seismic landslide inventories for spatial distribution analysis related to individual earthquakes

Date	Name	Mag.	Landslide number	Landslide area (km ²)	References
2008/5/12	Wenchuan, China	Mw 7.9	About 200,000	1,160	Xu et al. (2013b, c)
			About 48,000	712	Xu et al. (2009a, b)
			About 56,000	811	Dai et al. (2011)
			73,367	565.8	Parker et al. (2011)
			About 60,000	632	Gorum et al. (2011)
		43,842		Li et al. (2013)	
		<10,000		Qi et al. (2010)	
2005/10/8	Kashmir	Mw 7.6	2,252	61	Kamp et al. (2008)
			2,424		Sato et al. (2007)
			1,293		Owen et al. (2008)
2004/10/23	Mid-Niigata, Japan	Mw 6.6	4,400		Yamagishi and Iwahashi (2007)
			>1,000		Chigira and Yagi (2006)
			1,353		Sato et al. (2005)
			1,212	7.99	Wang et al. (2007)
1999/9/21	Chi-Chi, China Taiwan	Mw 7.5	9,272	127.8	Liao and Lee (2000); Liao et al. (2002); Lee et al. (2008)
			>10,000		Wang et al. (2003)
			>20,000		Wang et al. (2002)
1994/1/17	Northridge, California, USA	Mw 6.7	>11,000	23.8	Harp and Jibson (1995, 1996); Jibson and Harp (1994)
			100–1,000		Keefer et al. (2006)
2003/1/21	Tecomán, Mexico	Mw 7.6	1,000–10,000		Jibson et al. (2004)
2002/11/3	Denali fault, Alaska	Mw 7.9	About 200		Marzorati et al. (2002)
1997/9/26	Umbria-Marche	Mw 6.0	674		Fukuoka et al. (1997)
1995/1/17	Hyogo-ken, Japan	Mw 6.9	1,046		Keefer (2000)
1989/10/17	Loma Prieta, USA	Mw 6.9	100–1,000		Keefer et al. (1985)
1983/10/28	Borah Peak, Idaho	Mw 6.9	>7,400	200	Pearce and O'Loughlin (1985)
1929/6/17	Murchison	Mw 7.7	>220		Jibson and Keefer (1989)
1811/12/16	New Madrid, Mo.	Mw 8.3			

Table 2 Control factors of seismic landslides and their classifications

No.	Factor	Classification
1	Elevation/m	(1): <3,800; (2): 3,800–4,000; (3): 4,000–4,200; (4): 4,200–4,400; (5): 4,400–4,600; (6): 4,600–4,800; (7): 4,800–5,000; (8): >5,000
2	Slope°	(1): 0–5; (2): 5–10; (3): 10–15; (4): 15–20; (5): 20–25; (6): 25–30; (7): 30–35; (8): 35–40; (9): >40
3	Aspect	(1): Flat; (2): N; (3): NE; (4): E; (5): SE; (6): S; (7): SW; (8): W; (9): NW
4	Slope position	(1): Ridge; (2): upper slope; (3): middle slope; (4): flat slope; (5): lower slope; (6): valley
5	Distance from drainages/ m	(1): <100; (2): 100–200; (3): 200–300; (4): 300–400; (5): 400–500; (6): 500–600; (7): 600–700; (8): 700–800; (9): 800–900; (10): 900–1,000; (11): >1,000
6	Lithology	See Table 3
7	Distance from surface rupture/m	(1): 0–500; (2): 500–1,000; (3): 1,000–1,500; (4): 1,500–2,000; (5): 2,000–2,500; (6): 2,500–3,000; (7): 3,000–3,500; (8): 3,500–4,000; (9): 4,000–4,500; (10): 4,500–5,000; (11): 5,000–5,500; (12): 5,500–6,000; (13): 6,000–6,500; (14): 6,500–7,000; (15): 7,000–7,500; (16): 7,500–8,000; (17): 8,000–8,500; (18): 8,500–9,000; (19): 9,000–9,500; (20): 9,500–10,000; (21): >10,000
8	PGA/g	(1): >0.38; (2): 0.34–0.38; (3): 0.30–0.34; (4): 0.26–0.30; (5): 0.22–0.26; (6): 0.18–0.22; (7): 0.14–0.18; (8): <0.14

together form the boundary fault system of the of Bayan Har block (Fig. 2). The left-lateral slip for those ruptures along the Garzê-Yushu fault and the Eastern Kunlun fault and the reverse slip for the 2008 Wenchuan rupture along the Longmenshan thrust belt may indicate that the southeastward block motion controls the faulting behavior along its boundary fault system (Xu et al. 2010a). As of April 25, 2010 at 15:00 (Beijing time), 1,467 aftershocks were recorded, 13 aftershocks with magnitude $M_s \geq 3.0$, with the strongest measured as M_s 6.2 on April 14, 2010 at 09:25:17.8 (Beijing time).

3 Mapping of landslides triggered by the earthquake

At least 2,036 co-seismic landslides, with a total area of 1.194 km², were delineated by visual interpretation of aerial photographs and satellite images taken following the earthquake and verified by field inspection. We have tried to classify all the 2,036 landslides into different types based on remote sensing images but failed. Because many of the landslides were difficult to be classified even from remote sensing images in 0.2 and 0.4 m very high resolutions. For example, many landslides look like either rock falls or disrupted shallow landslides. Only some landslides we visited following the earthquake can be classified convincingly (Xu et al. 2013a). Therefore, the co-seismic landslides of all types are used for spatial distribution analysis.

Due to the large area of landslides, it is impossible to carry out detailed mapping on every landslide in the field. Rather the location and shape of each landslide are delineated by interpreting high-resolution color aerial photographs and remote sensing images, and such mapping is verified by field inspection. The remote sensing images we used are as follows: true color aerial photographs of 0.2 and 0.4 m resolution acquired by government agencies within several days after the earthquake; panchromatic satellite images of WorldView of 0.5 m resolution after the earthquake; multi-spectral SPOT 5 satellite images of 10 m resolution before and after the earthquake, and panchromatic SPOT 5 satellite images of 2.5 m resolution before and after the earthquake. About 100 landslide sites were visited in the field on foot or in a vehicle. Figure 3 shows two groups of aerial photographs and photos presenting co-seismic landslides occurrence. Before field investigations, a preliminary landslide inventory map was prepared by visual interpretation of remote sensing images. Then, after field investigations, the preliminary landslide inventory map was modified and a final inventory map was prepared. Due to the high resolution of the true color aerial photographs and satellite remote sensing images, almost all the landslides including small slope failures are mapped. The smallest landslide that is detectable has a superficial area of about 15 m². A spatial distribution map of the landslides is prepared on a GIS platform. In total, 2,036 landslides are plotted as individual polygons, and the centroids are extracted for mapping.

As shown in Fig. 2, the 2,036 landslides are distributed in an approximately rectangle of 1,455.3 km². The total superficial area of these landslides is about 1.194 km². Shallow and disrupted landslides are dominant, also including rock falls, deep-seated landslides, liquefaction-induced landslides, and compound landslides (Xu et al. 2013a). The main co-seismic surface rupture is in approximately alignment with the central line of the rectangle aforementioned (Fig. 2). Most of the co-seismic landslides occurred in clusters near the surface rupture belt.

The rectangular area containing the landslides is approximately between 32°52′6.7″N and 33°19′47.9″N latitude, and 96°20′32.9″E and 97°10′8.9″E longitude (Fig. 1). The length of the rectangle (parallel to the surface rupture, NW–SE trending) is 76.75 km, and

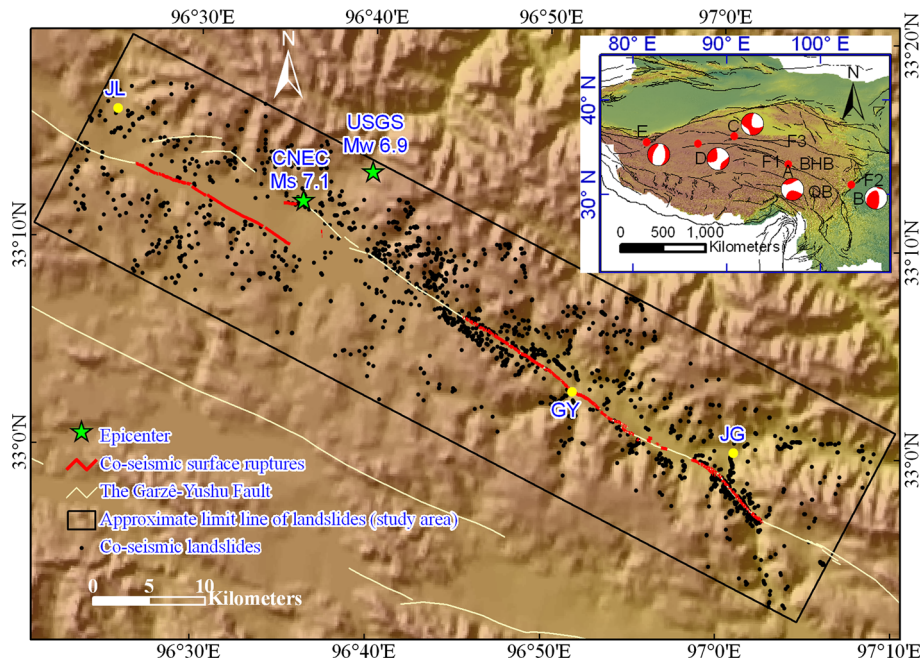


Fig. 2 Landslides triggered by the 2010 Yushu earthquake (revised after Xu et al. 2013a). Upper-right inset shows major events of or near Tibet in recent years. *a* Epicenter of the 2010 Mw 6.9 Yushu earthquake; *b* epicenter of the 2008 Mw 7.9 Wenchuan earthquake; *c* epicenter of the 2001 Mw 7.8 Kokoxili earthquake; *d* epicenter of the 1997 Mw 7.6 Manyi earthquake; *e* epicenter of the 2008 Mw 7.1 Yutian earthquake; *BHB* the Bayan Har block; *QB* Qiangtang block; *F1* the Xianshuihe fault zone, the Garzê-Yushu fault is a segment of the Xianshuihe fault; *F2* the Longmenshan thrust belt; *F3* the Eastern Kunlun fault; *JG* Jiegu Town, county station of the Yushu County; *JL* Jiulong Town; *GY* Guoyangyansongduo Village. Beach balls, indicating earthquake focal mechanisms, are downloaded from <http://www.globalcmt.org/CMTsearch.html>

its width is 18.96 km. Altitude in the study area ranges from 3,589.7 to 5,181.4 m. The natural slopes are relatively gentle, with an average slope gradient of 16.39°. And the proportion of area with slopes steeper than 30° is only 12 %.

Figure 4 shows LAP and LND grid cell maps of the earthquake. The LAP is defined as the percentage of the area affected by the landslides and LND is defined as the number of landslides per 1 km². We use 1 km × 1 km grid cells to perform statistical analysis of the landslide area and number density distributions in the study area. Figure 4 shows that the maximum LAP is 4.3625 %, and the largest LND value is 41 pieces/km². The average LAP and LND values within the study area are 0.082 % and 1.4 pieces/km², respectively. It also shows that landslides are concentrated along the co-seismic surface rupture.

4 Control factors of landslides

As stated earlier, the occurrence of landslides triggered by an earthquake is presumably controlled by several natural factors, such as elevation, slope angle, slope aspect, slope position, distance from drainages, lithology, distance from the surface rupture, and peak ground acceleration (PGA). We use LAP and LND analysis to study the correlation of

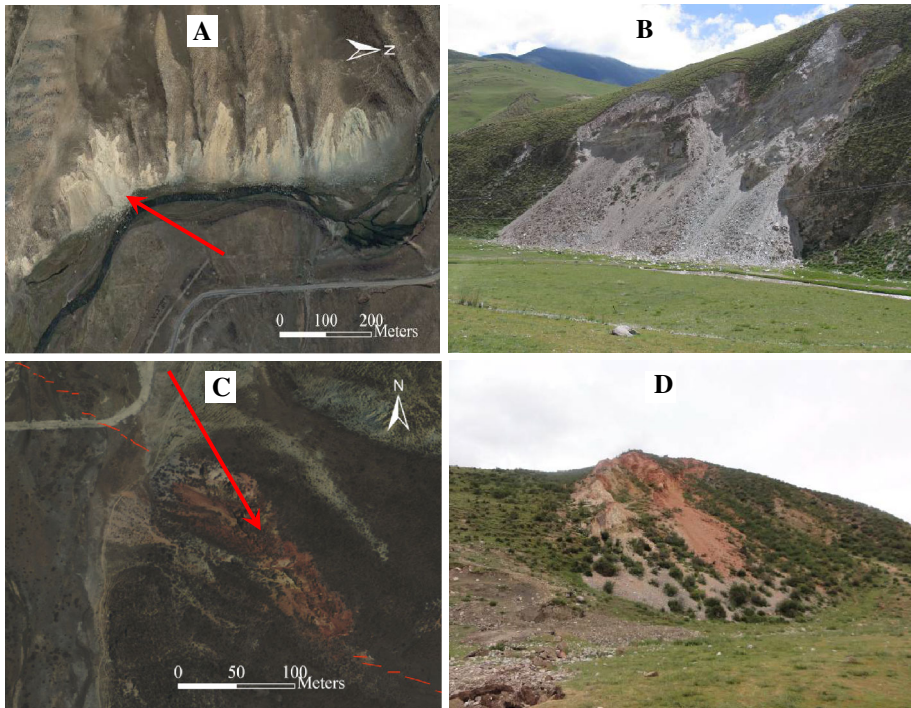


Fig. 3 Comparisons of aerial photographs and photos of two places where co-seismic landslides occurred. **a** Aerial photograph of a slope occurred clusters of rock falls; **b** field photo of some of the rock falls; **c** aerial photograph of a rock fall and **d** is field photo of the rock fall. *Red arrows* in **a** and **c** represent positions of camera and landslide targets. *Red thin lines* in **c** denote co-seismic surface ruptures

these control factors with the 2,036 landslides triggered by the Yushu earthquake. In the LND analysis, the centroids of the landslides are extracted from the landslide polygons, without considering of landslide scales. The analysis is carried out using a digital geological map compiled from 1:200,000-scale standard geological maps and digital topographic maps of a scale of 1:50,000. A digital elevation model (DEM) of a resolution of 5×5 m is produced using GIS software from the 1:50,000-scale topographic maps, with contour lines, contour points, and drainages.

4.1 Landslide concentration versus topographic parameters

Elevation differences and associated vegetation, weather, slope material moisture content, and seismic wave amplification effect can control seismic landslides. Classifications of elevation are given in Table 2. Figures 5a and 6a show the LAP and LND values in relation to the elevation. It can be seen that the highest LAP and LND values appear at elevations from 3,800 to 4,000 m.

The slope angles and slope aspects are taken from the DEM that has a resolution of 5 m. The slope angles are classified in an interval of 5° (Table 2). The slope angle is an essential impact parameter to co-seismic landslide occurrence. In general, the steeper the slope angle, the greater the decline force of the slope and thus the greater likelihood of landslide occurrence following a major earthquakes. As shown in Figs. 5b and 6b, both LAP and

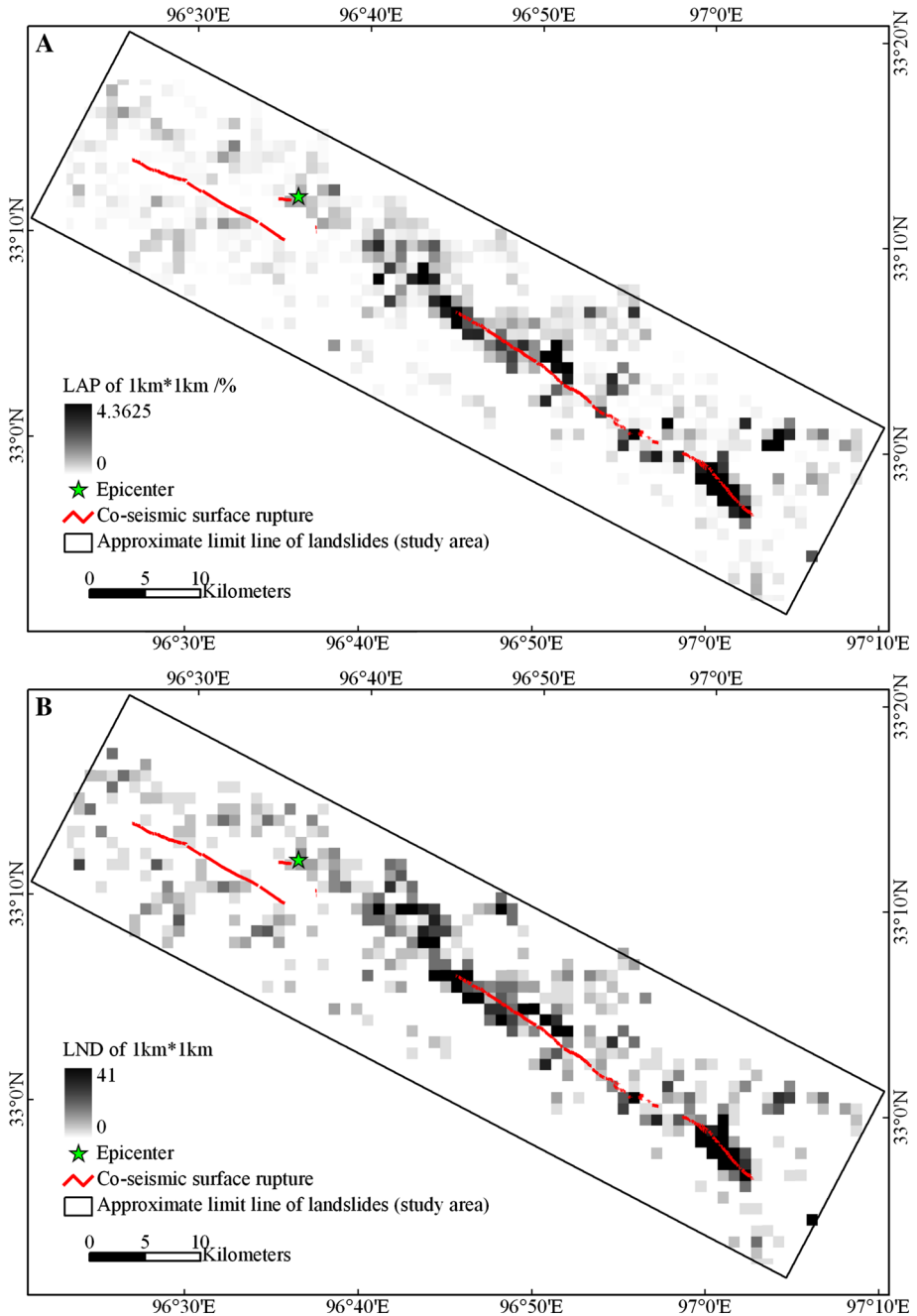


Fig. 4 Density maps of LAP and LND. **a** LAP density map; **b** LND density map

LND values increase with the slope angle, particularly for slopes exceeding 30°. Slope aspect is defined as the direction of maximum slope of the ground surface. The aspect of a slope is related to some factors such as exposure to sunlight, drying winds, rainfall (degree

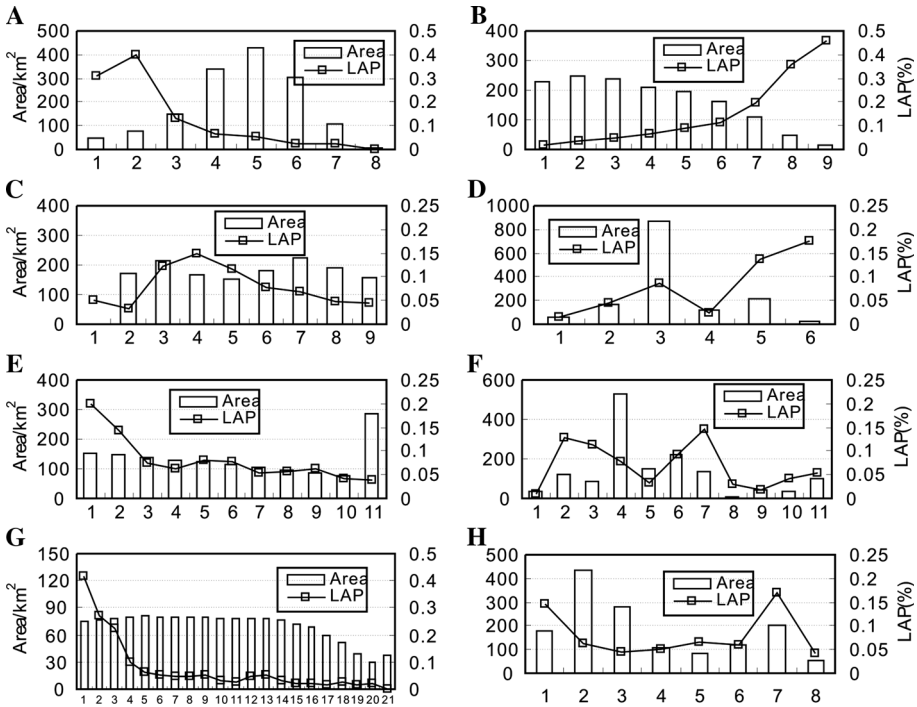


Fig. 5 LAP of eight control factors. **a** Elevation; **b** slope angle; **c** slope aspect; **d** slope position; **e** distance from drainages; **f** lithology; **g** distance from surface rupture; **h** PGA. The meanings of classification numbers were shown in Table 2

of saturation), and discontinuities that can control occurrence of seismic landslides (Yalcin 2008). It is also related to such factors as directional peak ground accelerations (Dai et al. 2011), and directions of seismogenic fault slipping and crust movement. The slope aspect is divided into nine classes for the study area, namely flat (horizontal), facing (dipping) N, NE, E, SE, S, SW, W, and NW (Table 2). Figures 5c and 6c show that NE-, E-, and SE-facing slopes are the favorite orientations for landslide occurrence. As these aspects corresponded to the sense of fault slip, likely related to the directivity of the seismogenic fault slip and seismic wave propagation.

The slope position is also a control factor of seismic landslides, as it determines spatial distribution of loose weathered material, topographic amplifying effect on seismic waves, and river effects on slope stability. Slope positions are classified into the categories of ridge, upper slope, middle slope, flat slope, lower slopes, and valleys (Table 2) (Weiss 2001). The slope position layer is extracted from the DEM based on the GIS platform. Both LAP and LND values (Figs. 5d, 6d) show that the lower the slope position, the higher the landslide occurrence, except for flat slopes which have values similar to that at the ridge crests.

As the undercutting action of a river may trigger instability of slopes, distances of landslides from drainages are also considered. The drainage map was extracted from the 1:50,000-scale topographic map and was used to construct the distance from drainages map. Buffer zone intervals for drainages were set to 100 m, and the distance from

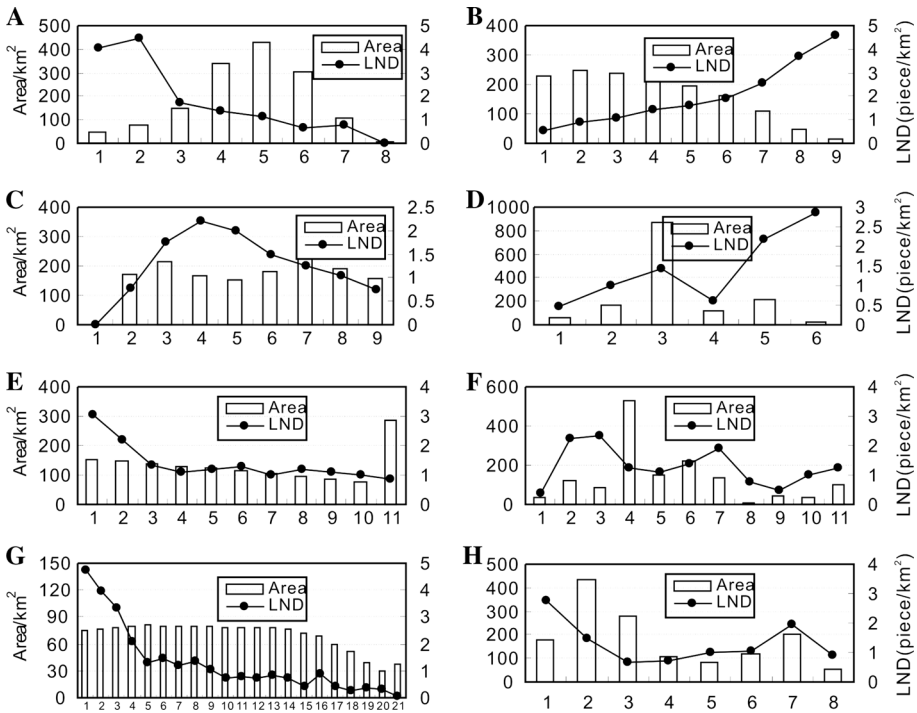


Fig. 6 LND of eight control factors. **a** Elevation; **b** slope angle; **c** slope aspect; **d** slope position; **e** distance from drainages; **f** lithology; **g** distance from surface rupture; **h** PGA. The meanings of classification numbers were shown in Table 2

drainages was comprised with 11 classes: 0–100, 100–200, 200–300, 300–400, 400–500, 500–600, 600–700, 700–800, 800–900, 900–1,000, and >1,000 m (as shown in Table 2). Both LAP and LND values decrease with increasing distance from drainages, but by far the greatest influence of this parameter is within the first 300 m from the drainages (Figs. 5e, 6e).

4.2 Landslide concentration versus geologic parameters

It is widely recognized that lithology plays an important role in co-seismic landslides occurrence, because strength structure, permeability, and composition, etc. of soil or rocks that constituting slopes determine the probability of landslide occurrence. From the geological map at a scale of 1:200,000 of the China Geological Survey (Fig. 7), the lithology of the study area is divided into eleven categories (Table 3): Q_4h , Q_4al-pl , N, T_3b , T_3kn^3 , T_3kn^2 , T_3kn^1 , T_2j^2 , T_2j^1 , C-P, and magmatic rocks. The lithology map, originally in vector format, is converted into raster format at 5×5 m resolution using the GIS software. As shown in Table 3 and Figs. 5f and 6f, the units Q_4al-pl , N, and T_3kn^1 (classes 2, 3, and 7) have higher LAP and LND than other units. The unit of N is composed of quartz sandstone, breccia, and T_3kn^1 unit is composed of feldspathic sandstone, siltstone, slate, limestone, phyllite, which have low shear strength and are heavily fractured. In addition, Q_4al-pl unit is composed of alluvium, fluvial deposits, and gravel, often distributed in valleys. Those places with these geological units are often landslide accumulation areas.

4.3 Landslide concentration versus earthquake parameters

Strong negative correlations are present between LAP and LND and the distance from main surface ruptures (Figs. 5g, 6g). The spatial distribution map (Fig. 2) shows that landslides are concentrated along the main seismic surface ruptures. Buffer zones for distance to the surface rupture are set to 500 m, and 21 intervals are obtained. Most landslides (1,187 landslides or 58.3 % of the total landslide number) occur within 2.5 km from the main surface ruptures. These landslides have an aggregate total area of 0.82 km² (68.8 % of the total), indicating that the landslides relatively close to the surface ruptures are on average also relatively larger. Few landslides occur more than 5 km from the surface ruptures.

In general, there was a good correlation between distribution of earthquake-triggered landslides and ground shaking. Values of peak ground acceleration (PGA) were derived from the US Geological Survey (2010) PGA map that used data from accelerometers, with interpolation based on both estimated amplitudes where data are lacking, and site amplification corrections. Most of the study area experienced high levels of ground shaking during the earthquake. A regional contour map of PGA from US Geological Survey (2010) indicates a range of PGA values of 0.12–0.38 g in the study area. There are eight classes of PGA values: 0.12, 0.16, 0.20, 0.24, 0.28, 0.32, 0.36, and 0.38 g. Figures 5h and 6h show the correlations of LAP and LND values with PGA. There is little apparent correlation between the LAP, LND, and PGA values, as increasing PGA values in general are not related to positive or consistent values of landslide occurrence. It is seen that the LAP and LND values decrease rapidly with a decrease of PGA values within the range of 0.38–0.32 g, but among the PGA values 0.32–0.16 g, the PGA values show an opposite

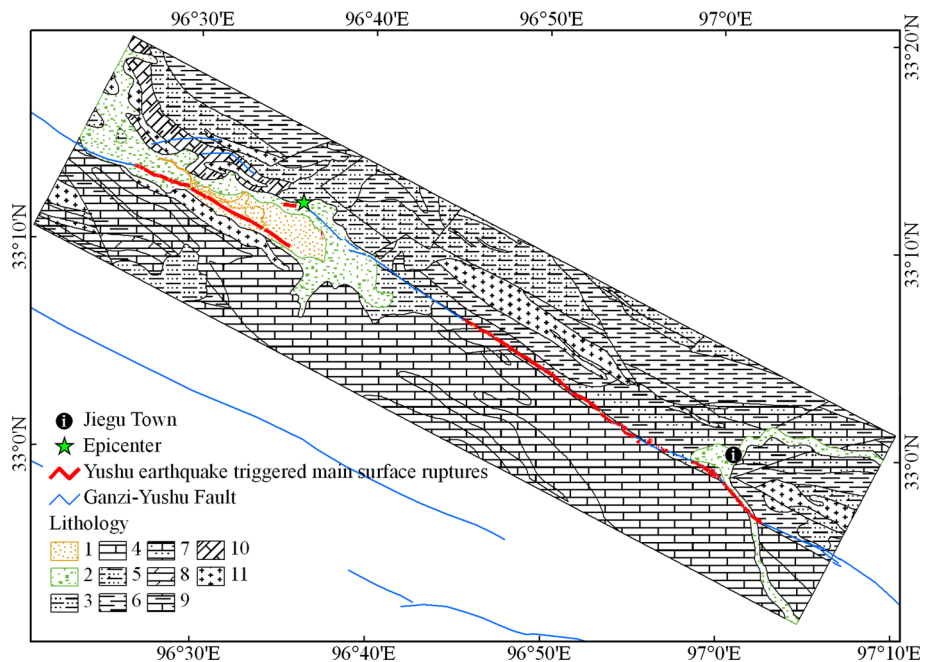


Fig. 7 Lithology map of the study area. The meanings of 1–9 are as in Table 3

Table 3 Geologic units and landslide occurrence in the study area

No.	Geologic unit	Description of lithology	Area/ km ²	Ls area/km ²	Ls number	LAP% (order)	LND/ls/km ² (order)
1	Q _{4h}	Lake silt, peat deposits	32.704	0.003	12	0.010 (11)	0.367 (11)
2	Q _{4al-pl}	Alluvium, fluvial deposits, and gravel	118.717	0.152	264	0.128 (2)	2.224 (2)
3	N	Quartz sandstone, breccia	84.382	0.096	198	0.114 (3)	2.346 (1)
4	T _{3br}	Limestone, quartz sandstone, siltstone, coarse sandstone, slate	530.217	0.412	652	0.078 (5)	1.230 (5)
5	T _{3kr³}	Quartz sandstone, siltstone, slate, mica schist	146.707	0.047	159	0.032 (8)	1.084 (7)
6	T _{3kr²}	Limestone, amphibolite schist, marble, metamorphic conglomerate	222.799	0.207	310	0.093 (4)	1.391 (4)
7	T _{3kr¹}	Feldspathic sandstone, siltstone, slate, limestone, phyllite	134.235	0.196	257	0.146 (1)	1.915 (3)
8	T _{2jl²}	Limestone	9.142	0.003	7	0.030 (9)	0.766 (9)
9	T _{2jl¹}	Slate, limestone, siltstone, quartz sandstone, conglomerate	42.796	0.008	21	0.019 (10)	0.491 (10)
10	C-P	Quartz sandstone, sandstone	34.628	0.015	35	0.043 (7)	1.011 (8)
11	Magmatic rocks	Quartz diorite, granite, diabase	98.974	0.054	121	0.055 (6)	1.223 (6)

Area area of certain lithology unit, *Ls area* landslide area in the unit, *Ls number* landslide number in the unit, *LAP* landslide area percentage of the unit, *LND* landslide number per area calculation unit

tendency. This result conforms to some previous case studies, such as the Wenchuan earthquake (Xu et al. 2010b) and the Northridge earthquakes (Parise and Jibson 2000), in which severity of shaking not necessarily shows clear correlation with landslide occurrence.

5 Landslide distribution on both sides of the surface rupture

The aim of this section was to carry out research on the spatial distribution difference of landslides triggered on the two sides of the fault. The strike of the main co-seismic surface rupture of the Yushu event is about 300° . The study area is divided into two parts by the main rupture. The two parts are designated as the North (N-) side and the South (S-) side, respectively. The N-side occupies an area of 759.99 km^2 , and the S-side comprises an area of 695.31 km^2 . On the N-side, there are 1,172 landslides with a total area of 0.695 km^2 , the average area of one landslide 584.4 m^2 ; the LAP is 0.09 % and LND is 1.542 pieces/ km^2 . On the S-side, there are 864 landslides with a total area of 0.509 km^2 ; average area of one landslide is 589.2 m^2 ; the LAP is 0.073 % and LND is 1.243 pieces/ km^2 . Thus, more landslides occur on the North side, and the landslide area, LAP, and LND are all relatively larger there.

The same eight control factors are used to compare landslide distributions on the N-side and S-side. Topographically, elevations on the North side range from 3,589.71 to 5,181.36 m, with an average of 4,415.55 m, and those on the South side ranged from 3,706.53 to 4,969.05 m, with an average of 4,439.85 m. The area distributions of elevations on the two sides are shown in Figs. 8a and 9a, respectively. Slope angles on the North side ranged from 0° to 61.27° , with an average of 18.57° , and those on South side range from 0° to 50.58° , with an average of 14.01° , so the slope of North side is steeper on average than the South side. The area distributions of slope angles on the two sides are shown in Figures 8b, and 9b. PGA values on the North side range from 0.12 to 0.38 g, with an average of 0.289 g, and those on the South side also ranged from 0.12 to 0.38 g, with an average of 0.2968 g. The area distributions of PGA for the two sides are shown in Figs. 8h and 9h, respectively. The area distributions of other five impact factors are shown in Figs. 8c–g and 9c–g.

Landslide area percentage and LND values in all intervals of each factor on the two sides of the rupture are compared (Figs. 8, 9). Both LAP and LND are largely similar on either side for each interval and in the individual factor ranks though with a few exceptions. For example, the landslide spatial distribution for elevation and slope angle are somewhat different on the two sides. For elevations of 3,800–4,000 m, the LAP on the South side is about 0.3 % more than on the North side, and the LND on the South side is about 5 pieces/ km^2 greater than on the North side. For slope angles over 30° , the LAP of the South side is about 0.4 % more than of the North side, and the LND of South side is about 4.5 pieces/ km^2 higher than of the North side. Also, The LAP and LND decaying with distance from the surface rupture on the South side are more rapid than on the North side.

We infer that two reasons account for landslide number, landslide area, LAP, and LND on the North side being higher than on the South side. Firstly, the average slope angle on the North side (18.57°) is greater than on the South side (14.01°). There were the tectonic activity differences of the two sides: the North side is located on the Bayan Har block, which has experienced several big earthquakes whereas the South side is located on the Qiangtang block, which is more quietly and less earthquake events along its boundary in recent decades. These large earthquakes (Fig. 2) including the May 12, Wenchuan Mw 7.9

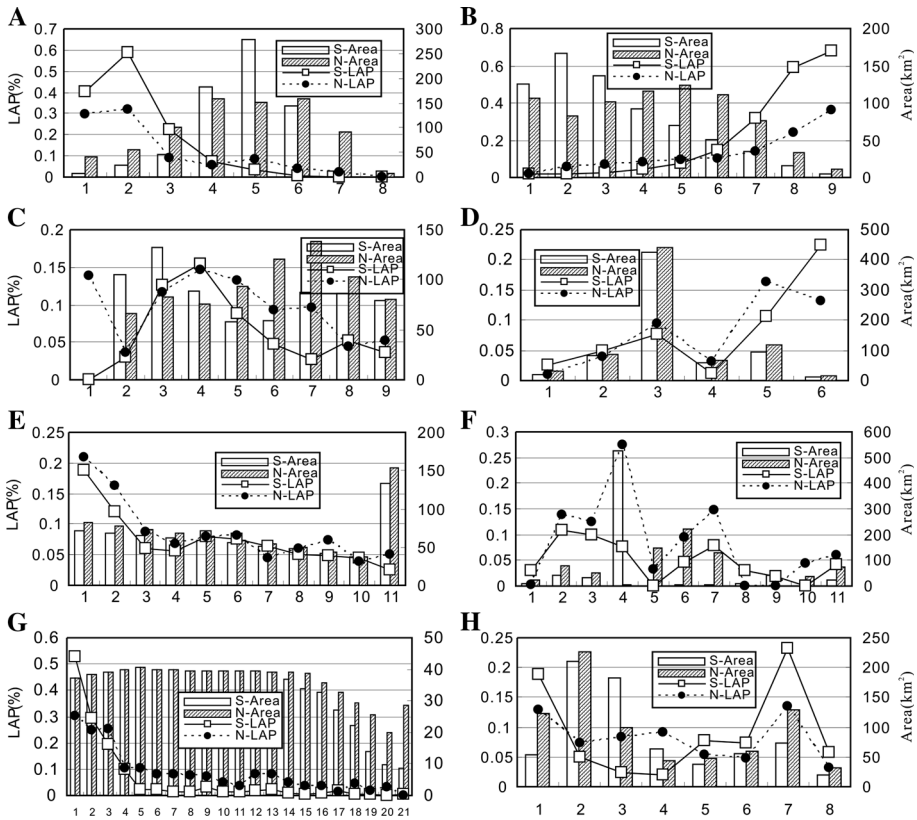


Fig. 8 LAP values of on either side of surface rupture versus control factors. **a** Elevation; **b** slope angle; **c** slope aspect; **d** slope position; **e** distance from drainages; **f** Lithology; **g** distance from surface rupture; **h** PGA. The meanings of classification numbers were shown in Table 2

earthquake, the March 21, 2008 Yutian Mw 7.1 earthquake, the November 14, 2001 Kokoxili Mw 7.8 earthquake, and the November 8, 1997 Manyi Mw 7.6 earthquake (Xu et al. 2013f). Nevertheless, the spatial distributions of landslides triggered by the Yushu earthquake are largely similar on either side of the surface rupture.

6 Comparing the influence of five control factors on landslides

We use a bivariate statistical method (Xu and Xu 2013; Xu et al. 2013b) for comparing the influence of five control factors on the landslides. In this method, a percentage value of an impact parameter decided by spatial distribution of landslides is derived, which implies the spatial distribution intensity of co-seismic landslides. In Fig. 10, the horizontal axis means cumulative percentage of class area, and vertical axis means the corresponding cumulative percentage of the co-seismic landslide area (landslide area in a class divided by the total landslide area). The effects of elevation, slope aspect, and slope position on landslide occurrence are complex and may depend on other factors. So, the other five impact factors—slope angle, distance from drainages, lithology, distance from surface rupture, and

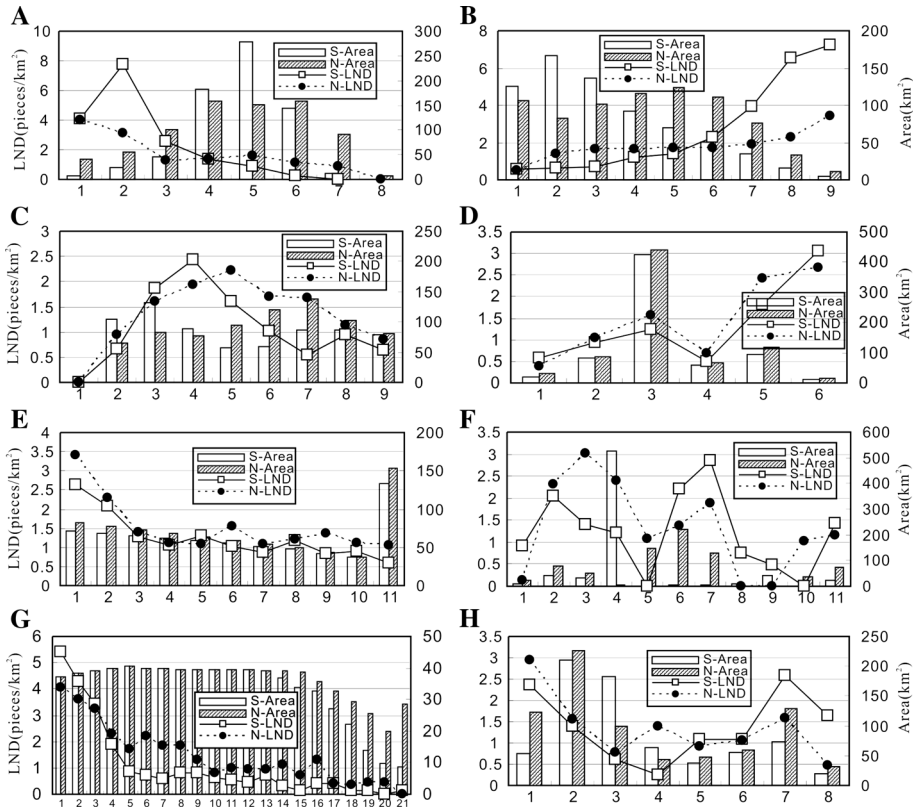
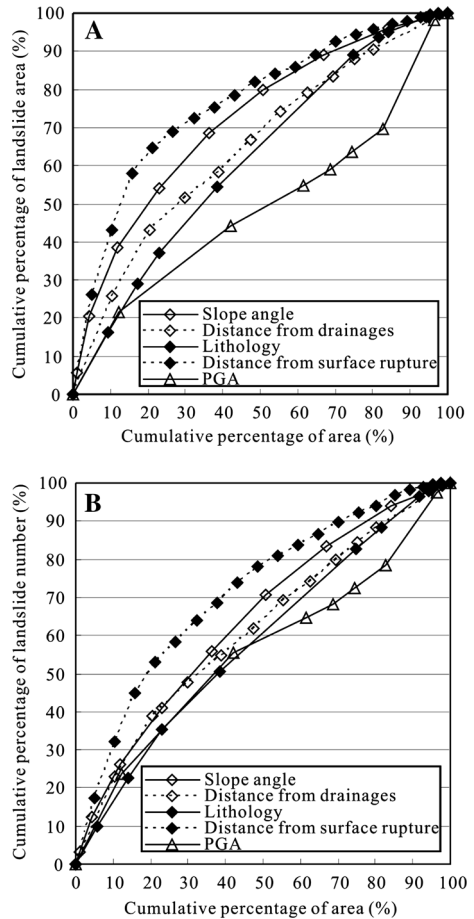


Fig. 9 LND values of on either side of surface rupture versus control factors. **a** Elevation; **b** slope angle; **c** slope aspect; **d** slope position; **e** distance from drainages; **f** lithology; **g** distance from surface rupture; **h** PGA. The meanings of classification numbers were shown in Table 2

PGA—are selected for this analysis. We assume that these five factors are conditionally independent of one another with respect to the earthquake-triggered landslides. The descending curves of cumulative LAP and LND are determined. In general, these factors of slope angle, distance from drainages, distance from surface rupture, and PGA have positive correlations with landslide occurrence. So the cumulative curves of these factors are constructed from the steepest slope angle interval ($>40^\circ$), the nearest distance from drainages interval (<100 m), the nearest distance from the surface rupture interval (<500 m), and the high PGA value (>0.38 g). The lithology, as a discrete factor, and the ordering of LAP and LND with respect to lithology are shown in Table 3. The cumulative percentage area curves for lithology are constructed by the ordering from 1 to 11 of LAP and LND, respectively (Fig. 10). The area under the cumulative curve (AUC) is used as the contrast index for comparing the influence on landslides.

The comparison results of LAP and LND AUC values of these control factors (Table 4) show that the distance from the surface rupture has the greatest impact on earthquake landslides, followed by slope angle. For both the LAP and LND AUC values, the descending order of the five impact factors are the distance from surface rupture $>$ slope angle $>$ distance from drainages $>$ lithology $>$ PGA. The PGA perhaps has no significant

Fig. 10 Cumulative percentages of area and versus cumulative percentage landslide for five impact factors. **a** Landslide area; **b** landslide number



effect on the Yushu earthquake landslides as we stated previously. Probably, it is because the strong ground motion marked by PGA contributes primarily to triggering landslides, while other factors control the distribution of landslides in the study area.

7 Landslide size and morphometric parameters

The cumulative number–area relationship for landslides can be represented as the following relationship (also be presented in Dai et al. 2011; Chigira et al. 2010 for the 2008 Wenchuan earthquake-triggered landslides), which states that the logarithm of the number N of landslides exceeding a given area A is linearly related to the area:

$$\text{Log}_{10}N(A) = a + b \text{Log}_{10}A,$$

where $N(A)$ is the cumulative number of landslides whose area is larger than or equal to A , A is the area of one landslide, and a and b are constants. As shown in Fig. 11a, at small areas the curve bends toward the horizontal line. Figure 11b shows the relationship of landslide number and landslide area. The landslide area range division selects a power of

Table 4 AUC values of landslide area and landslide number

Impact factor	AUC for area	AUC for number	Ordering
Slope angle	71.82	64.08	2
Distance from drainages	64.44	61.28	3
Lithology	61.73	58.31	4
Distance from surface rupture	76.26	71.27	1
PGA	45.48	52.18	5

AUC area under curve

two (Table 5). Figure 11a, b shows it is much difficult to obtain a rigorously complete sample for small landslides.

Simple morphometric parameters including the length, width, and aspect ratio are analyzed. Length (the horizontal distance from the crown of a landslide to its tip) is computed along the direction of landslide movement. Width is measured as the average width, calculated as the area divided by length. Lengths of the earthquake landslides range from 6 to more than 415 m with an average of about 40 m. Landslide widths range from 1.7 to 76.7 m with an average of 10.8 m. The shape of a landslide can be described by its aspect ratio (length/width) (Parise and Jibson 2000). A low aspect ratio is typical of a rotational landslide. When the length is much greater than the width, and the ratio thus is greater, the elongated shape is typical of both flow-type landslides and disrupted slides, which have long to very long runout distances (Parise and Jibson 2000). Landslide ratios for the Yushu earthquake landslides range from 1.5 to 32.8 with an average of 4.15. This result is greater than the ratios of landslides (a mean ratio of 2.6 for single landslides and 1.2 for landslides complexes) triggered by the January 17, 1994 Northridge, California M 6.7 earthquake (Parise and Jibson 2000). Figure 12 shows the correlation between landslide ratios and landslide numbers. The ratios of most landslides (1,726 landslides, 84.8 % of the total landslides) are <6.

8 Discussion

The spatial distribution area of the co-seismic landslides triggered by the Yushu earthquake is about 1,500 km². Keefer (1984) has constructed a loose correlation between earthquake magnitude and co-seismic landslides considering individual earthquake events before 1980 worldwide. Later, Rodríguez et al. (1999) added some new earthquake events during 1980–1997 and made a slight change to the loose correlation (Fig. 13). In addition, we supplement some other earthquakes in recent years (mainly shown in Table 1). In order to compare co-seismic landslides distribution area related to the Yushu earthquake with other events worldwide, a point corresponding to magnitude of Mw 6.9 and 1,500 km² of the landslide spatial distribution area is plotted on Fig. 13. It can be observed that the landslide spatial distribution area related to the Yushu earthquake is within the two upper margins determined by Keefer (1984) and Rodríguez et al. (1999). And the location of the Yushu earthquake in the Fig. 13 shows a moderate area affected by co-seismic landslides. In addition, considering very high resolutions of aerial photographs and satellite images used for the Yushu earthquake, the detailed and comprehensive level of the inventory of the Yushu earthquake-triggered landslides would be higher than other earlier earthquake

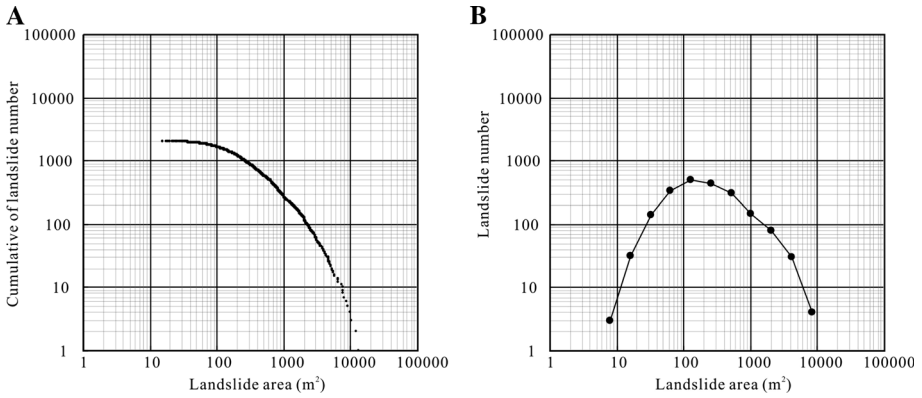


Fig. 11 Correlations between landslide frequency and the landslide area. **a** Cumulative landslide number; **b** landslide number

Table 5 Selected points of cumulative of landslide number

No.	Range of landslide area/km ²	Landslide number (frequency)
1	<16	3
2	[16, 32)	32
3	[32, 64)	140
4	[64, 128)	341
5	[128, 256)	500
6	[256, 512)	447
7	[512, 1,024)	308
8	[1,024, 2,048)	149
9	[2,048, 4,096)	81
10	[4,096, 8,192)	29
11	≥8,192	6
Total		2,036

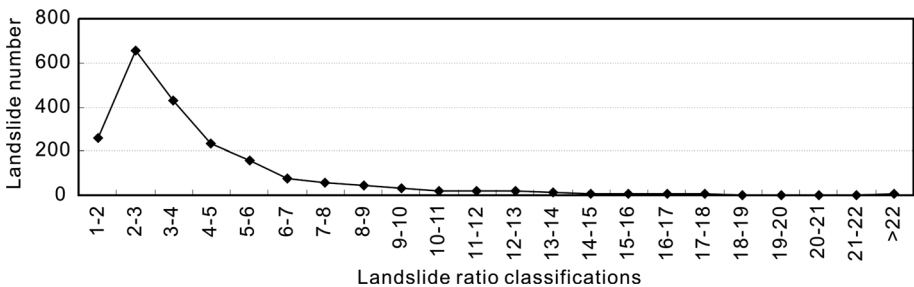


Fig. 12 Co-seismic landslide aspect ratio (length/width) distribution

events. Therefore, we consider the density, area, and scales of co-seismic landslides triggered by the Yushu earthquake are less than those of the other earthquakes of similar magnitudes if quality differences of remote sensing data are excluded. The main probable

reason is due to the seismogenic fault of the Yushu earthquake is a strike-slipping fault, rather than a thrust fault. Generally, landslides triggered by thrusting earthquakes (e.g., the 2005 Kashmir earthquake, the 1999 Chi-Chi earthquake, and the Wenchuan earthquake, see Table 1) are often much more serious than that of strike-slip earthquakes (e.g., the 2001 Kokoxili, China earthquake, van der Woerd et al. 2004).

A previous publication (Xu et al. 2013a) mainly focused on field investigation, classifications, and mechanisms of the landslides triggered by the earthquake. Although there was a section about spatial distribution analysis of landslides triggered by the earthquake, it is very simple. In this paper, we focus on landslides spatial distribution analyses, especially analyzing spatial distribution differences on two sides of the co-seismic surface rupture, and comparison of controlling factors. These studies are rare seen for previous other earthquake events. We found that the landslides spatial distribution of both sides of the seismogenic fault for the Yushu event has rather different patterns from that of thrusting-fault earthquakes, such as the 2008 Wenchuan earthquake, the 1999 Chi-Chi earthquake, and the 2005 Kashmir earthquake. These differences remind us that we should take different strategies of earthquake-landslide prevention and mitigation for the events with different seismogenic mechanisms.

9 Conclusions

We have mapped 2,036 landslides caused by the 2010 Mw 6.9 Yushu earthquake from visual interpreting of aerial photographs and satellite images and field inspection. Density maps of LAP and LND are constructed. It is found that most of the landslides are concentrated along the major surface rupture produced by this event. Landslide occurrence has a positive correlation with the slope angle, and negative correlations with distance from the surface rupture, and distance from drainages. The highest LAP and LND values appear at

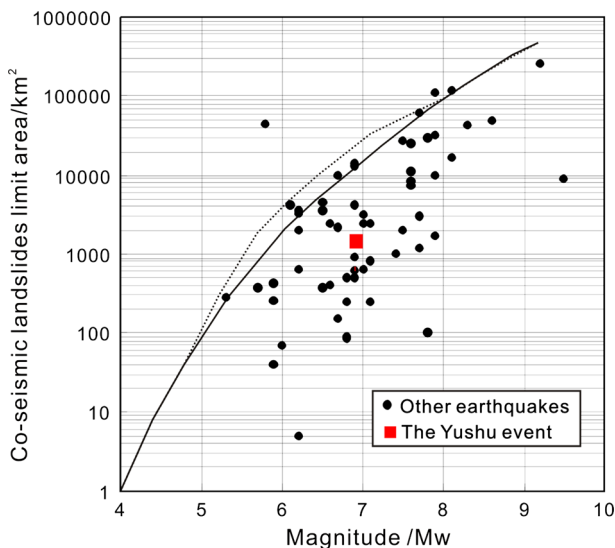


Fig. 13 Correlations between co-seismic landslide limit areas and earthquake magnitude (M_w) worldwide. The *solid line* is from Keefe (1984) and the *dashed line* is from Rodríguez et al. (1999)

places of elevations from 3,800 to 4,000 m. The distributions of the landslides are dominated by NE, E, and SE directions. The “valleys” on slopes are the most susceptible to landslides, and three geologic formation units, designated as Q_4al-pl , N, and T_3kn^1 , host the most concentrated earthquake landslides. No apparent correlations are found between LAP and LND and PGA values. On either side of the surface rupture, the spatial distributions of landslides are largely similar, though with a few exceptions, which is related to the nature of the strike-slip seismogenic fault. The bivariate statistical analysis for comparing the influence of various parameters on landslide occurrence show that, in descending order, the degrees of relative influence of the factors on landslides are the distance from the surface rupture > slope angle > distance from drainages > lithology > PGA. As for morphometric parameters, the aspect ratios (length/width) of most landslides (1,726 landslides, 84.8 % of the total landslides) are generally <6.

Acknowledgments This work was supported by the National Science Foundation of China (41202235 and 91214201). The authors would like to express their sincere thanks to David K. Keefer for his help in improvement of the manuscript.

References

- Chen LC, Wang H, Ran YK, Sun XZ, Su GW, Wang J, Tan XB, Li ZM, Zhang XQ (2010) The Ms 7.1 Yushu earthquake surface rupture and large historical earthquakes on the Garzê-Yushu Fault. *Chin Sci Bull* 55(31):3504–3509. doi:[10.1007/s11434-010-4079-2](https://doi.org/10.1007/s11434-010-4079-2)
- Chigira M, Yagi H (2006) Geological and geomorphological characteristics of landslides triggered by the 2004 Mid Niigata prefecture earthquake in Japan. *Eng Geol* 82(4):202–221. doi:[10.1016/j.enggeo.2005.10.006](https://doi.org/10.1016/j.enggeo.2005.10.006)
- Chigira M, Wu XY, Inokuchi T, Wang GH (2010) Landslides induced by the 2008 Wenchuan earthquake, Sichuan, China. *Geomorphology* 118(3–4):225–238. doi:[10.1016/j.geomorph.2010.01.003](https://doi.org/10.1016/j.geomorph.2010.01.003)
- Dai FC, Xu C, Yao X, Xu L, Tu XB, Gong QM (2011) Spatial distribution of landslides triggered by the 2008 Ms 8.0 Wenchuan earthquake, China. *J Asian Earth Sci* 40(4):883–895. doi:[10.1016/j.jseas.2010.04.010](https://doi.org/10.1016/j.jseas.2010.04.010)
- Fukuoka H, Sassa K, Scarascia-Mugnozza G (1997) Distribution of landslides triggered by the 1995 Hyogoken Nanbu earthquake and long runout mechanism of the Takarazuka Golf Course landslide. *J Phys Earth* 45(2):83–90
- Gorum T, Fan XM, van Westen CJ, Huang RQ, Xu Q, Tang C, Wang GH (2011) Distribution pattern of earthquake-induced landslides triggered by the 12 May 2008 Wenchuan earthquake. *Geomorphology* 133(3–4):152–167. doi:[10.1016/j.geomorph.2010.12.030](https://doi.org/10.1016/j.geomorph.2010.12.030)
- Harp EL, Jibson RW (1995) Inventory of landslides triggered by the 1994 Northridge, California earthquake. US Geol Surv Open-File Rep 95–213:17
- Harp EL, Jibson RW (1996) Landslides triggered by the 1994 Northridge, California, earthquake. *Bull Seimol Soc Am* 86(1B):S319–S332
- Harp EL, Keefer DK, Sato HP, Yagi H (2011) Landslide inventories: the essential part of seismic landslide hazard analyses. *Eng Geol* 122(1–2):9–21. doi:[10.1016/j.enggeo.2010.06.013](https://doi.org/10.1016/j.enggeo.2010.06.013)
- Jiang HC, Mao X, Xu HY, Yang HL, Ma XL, Zhong N, Li YH (2013) Provenance and earthquake signature of the last deglacial Xinmocun lacustrine sediments at Diexi, East Tibet. *Geomorphology*. doi:[10.1016/j.geomorph.2013.08.032](https://doi.org/10.1016/j.geomorph.2013.08.032)
- Jibson RW, Harp EL (1994) Landslides triggered by the Northridge earthquake. *Earthq Volcanoes* 25(1):31–41
- Jibson RW, Keefer DK (1989) Statistical analysis of factors affecting landslide distribution in the new Madrid seismic zone, Tennessee and Kentucky. *Eng Geol* 27(1–4):509–542. doi:[10.1016/0013-7952\(89\)90044-6](https://doi.org/10.1016/0013-7952(89)90044-6)
- Jibson RW, Harp EL, Schulz W, Keefer DK (2004) Landslides triggered by the 2002 Denali Fault, Alaska, earthquake and the inferred nature of the strong shaking. *Earthq Spectra* 20(3):669–691. doi:[10.1193/1.1778173](https://doi.org/10.1193/1.1778173)
- Kamp U, Growley BJ, Khattak GA, Owen LA (2008) GIS-based landslide susceptibility mapping for the 2005 Kashmir earthquake region. *Geomorphology* 101(4):631–642. doi:[10.1016/j.geomorph.2008.03.003](https://doi.org/10.1016/j.geomorph.2008.03.003)

- Keefer DK (1984) Landslides caused by earthquakes. *Geol Soc Am Bull* 95(4):406–421. doi:[10.1130/0016-7606\(1984\)95<406:LCBE>2.0.CO;2](https://doi.org/10.1130/0016-7606(1984)95<406:LCBE>2.0.CO;2)
- Keefer DK (2000) Statistical analysis of an earthquake-induced landslide distribution—the 1989 Loma Prieta, California event. *Eng Geol* 58(3–4):231–249. doi:[10.1016/S0013-7952\(00\)00037-5](https://doi.org/10.1016/S0013-7952(00)00037-5)
- Keefer DK, Wilson RC, Harp EL, Lips EW (1985) The Borah Peak, Idaho earthquake of October 28, 1983-landslides. *Earthq Spectra* 2(1):91–125. doi:[10.1193/1.1585304](https://doi.org/10.1193/1.1585304)
- Keefer DK, Wartman J, Ochoa CN, Rodriguez-Marek A, Wieczorek GF (2006) Landslides caused by the M 7.6 Tecoman, Mexico earthquake of January 21, 2003. *Eng Geol* 86(2–3):183–197. doi:[10.1016/j.enggeo.2006.02.017](https://doi.org/10.1016/j.enggeo.2006.02.017)
- Lee CT, Huang CC, Lee JF, Pan KL, Lin ML, Dong JJ (2008) Statistical approach to earthquake-induced landslide susceptibility. *Eng Geol* 100(1–2):43–58. doi:[10.1016/j.enggeo.2008.03.004](https://doi.org/10.1016/j.enggeo.2008.03.004)
- Li WL, Huang RQ, Tang C, Xu Q, van Westen C (2013) Co-seismic landslide inventory and susceptibility mapping in the 2008 Wenchuan earthquake disaster area, China. *J Mt Sci* 10(3):339–354. doi:[10.1007/s11629-013-2471-5](https://doi.org/10.1007/s11629-013-2471-5)
- Liao HW, Lee CT (2000) Landslides triggered by the Chi-Chi earthquake. *Proceedings of the 21st Asian Conference on Remote Sensing, Taipei*, 1–2, pp 383–388
- Liao C, Liao H, Lee C (2002) Statistical analysis of factors affecting landslides triggered by the 1999 Chi-Chi earthquake, Taiwan. *American Geophysical Union, Fall Meeting 2002*, abstract #H12D-0951
- Marzorati S, Luzzi L, Amicis MD (2002) Rock falls induced by earthquakes: a statistical approach. *Soil Dyn Earthq Eng* 22(7):565–577. doi:[10.1016/S0267-7261\(02\)00036-2](https://doi.org/10.1016/S0267-7261(02)00036-2)
- Meunier P, Uchida T, Hovius N (2013) Landslide patterns reveal the sources of large earthquakes. *Earth Planet Sci Lett* 363:27–33. doi:[10.1016/j.epsl.2012.12.018](https://doi.org/10.1016/j.epsl.2012.12.018)
- Owen LA, Kamp U, Khattak GA, Harp EL, Keefer DK, Bauer MA (2008) Landslides triggered by the 8 October 2005 Kashmir earthquake. *Geomorphology* 94(1–2):1–9. doi:[10.1016/j.geomorph.2007.04.007](https://doi.org/10.1016/j.geomorph.2007.04.007)
- Pan J, Li H, Xu Z, Li N, Wu F, Guo R, Zhang W (2010) Surface rupture characteristics and rupture mechanics of the Yushu earthquake (Ms7.1), 14/04/2010. *American Geophysical Union, Fall Meeting 2010*, abstract #T54B-08
- Parise M, Jibson RW (2000) A seismic landslide susceptibility rating of geologic units based on analysis of characteristics of landslides triggered by the 17 January, 1994 Northridge, California earthquake. *Eng Geol* 58(3–4):251–270. doi:[10.1016/S0013-7952\(00\)00038-7](https://doi.org/10.1016/S0013-7952(00)00038-7)
- Parker RN, Densmore AL, Rosser NJ, de Michele M, Li Y, Huang RQ, Whadcoat S, Petley DN (2011) Mass wasting triggered by 2008 Wenchuan earthquake is greater than orogenic growth. *Nat Geosci* 4(7):449–452. doi:[10.1038/ngeo1154](https://doi.org/10.1038/ngeo1154)
- Pearce AJ, O'Loughlin CL (1985) Landsliding during a M 7.7 earthquake: influence of geology and topography. *Geology* 13(12):855–858. doi:[10.1130/0091-7613\(1985\)13<855:LDAMEI>2.0.CO;2](https://doi.org/10.1130/0091-7613(1985)13<855:LDAMEI>2.0.CO;2)
- Qi SW, Xu Q, Lan HX, Zhang B, Liu JY (2010) Spatial distribution analysis of landslides triggered by 2008.5.12 Wenchuan Earthquake, China. *Eng Geol* 116(1–2):95–108. doi:[10.1016/j.enggeo.2010.07.011](https://doi.org/10.1016/j.enggeo.2010.07.011)
- Rodríguez CE, Bommer JJ, Chandler RJ (1999) Earthquake-induced landslides: 1980–1997. *Soil Dyn Earthq Eng* 18(5):325–346. doi:[10.1016/S0267-7261\(99\)00012-3](https://doi.org/10.1016/S0267-7261(99)00012-3)
- Sato HP, Sekiguchi T, Kojiro R, Suzuki Y, Lida M (2005) Overlaying landslides distribution on the earthquake source, geological and topographical data: the Mid Niigata prefecture earthquake in 2004, Japan. *Landslides* 2(2):143–152. doi:[10.1007/s10346-005-0053-5](https://doi.org/10.1007/s10346-005-0053-5)
- Sato HP, Hasegawa H, Fujiwara S, Tobita M, Koarai M, Une H, Iwahashi J (2007) Interpretation of landslide distribution triggered by the 2005 Northern Pakistan earthquake using SPOT 5 imagery. *Landslides* 4(2):113–122. doi:[10.1007/s10346-006-0069-5](https://doi.org/10.1007/s10346-006-0069-5)
- U. S. Geological Survey (2010) Advanced national seismic system (ANSS), shake map, global region, maps of ground shaking and intensity for event 2010 yr, Southern Qinghai, China. <http://earthquake.usgs.gov/eqcenter/shakemap>
- van der Woerd J, Owen LA, Tapponnier P, Xu XW, Kervyn F, Finkel RC, Barnard PL (2004) Giant, ~M8 earthquake-triggered ice avalanches in the eastern Kunlun Shan, northern Tibet: characteristics, nature and dynamics. *Geol Soc Am Bull* 116(3–4):394–406. doi:[10.1130/B25317.1](https://doi.org/10.1130/B25317.1)
- Wang WN, Nakamura H, Tsuchiya S, Chen CC (2002) Distributions of landslides triggered by the Chi-Chi Earthquake in Central Taiwan on September 21, 1999. *Landslides* 38(4):18–26
- Wang WN, Wu HL, Nakamura H, Wu SC, Ouyang S, Yu MF (2003) Mass movements caused by recent tectonic activity: the 1999 Chi-Chi earthquake in central Taiwan. *Isl Arc* 12(4):325–334. doi:[10.1046/j.1440-1738.2003.00400.x](https://doi.org/10.1046/j.1440-1738.2003.00400.x)

- Wang HB, Sassa K, Xu WY (2007) Analysis of a spatial distribution of landslides triggered by the 2004 Chuetsu earthquakes of Niigata Prefecture, Japan. *Nat Hazards* 41(1):43–60. doi:[10.1007/s11069-006-9009-x](https://doi.org/10.1007/s11069-006-9009-x)
- Weiss AD (2001) Topographic position and landforms analysis. www.jennessent.com/downloads/tpi-poster-tnc_18x22.pdf
- Wu FY, Li H, Pan J, Xu Z, Li N, Guo R, Zhang W (2010) Field measurements along the 2010 Ms 7.1 Yushu earthquake rupture shows strike-slip and dip-slip activities, resulting in mountains uplift. American Geophysical Union, Fall Meeting 2010, abstract #T51B-2033
- Xu C, Xu XW (2013) Controlling parameter analyses and hazard mapping for earthquake triggered-landslides: an example from a square region in Beichuan County, Sichuan Province, China. *Arab J Geosci* 6(10):3827–3839. doi:[10.1007/s12517-012-0646-y](https://doi.org/10.1007/s12517-012-0646-y)
- Xu C, Dai FC, Yao X (2009a) Incidence number and affected area of Wenchuan earthquake-induced landslides. *Sci Technol Rev* 27(11):79–81 (in Chinese)
- Xu C, Dai FC, Chen J, Tu XB, Xu L, Li WC, Tian W, Cao YB, Yao X (2009b) Identification and analysis of secondary geological hazards triggered by a magnitude 8.0 Wenchuan earthquake. *J Remote Sens* 13(4):745–753
- Xu XW, Yu GH, Sun XZ (2010a) Yushu earthquake slip: implication of great earthquake migration along boundary fault system of Bayan Har block, Tibetan Plateau. American Geophysical Union, Fall Meeting 2010, abstract #T22A-04
- Xu C, Dai FC, Yao X, Chen J, Tu XB, Xiao JZ, Sun Y (2010b) Study on the distribution of landslides triggered by the May 12, 2008 Wenchuan earthquake in two square typical regions. *J Grad Sch Chin Acad Sci* 27(5):621–630 (in Chinese)
- Xu C, Dai FC, Xu XW, Lee YH (2012a) GIS-based support vector machine modeling of earthquake-triggered landslide susceptibility in the Jianjiang River watershed, China. *Geomorphology* 145–146:70–80. doi:[10.1016/j.geomorph.2011.12.040](https://doi.org/10.1016/j.geomorph.2011.12.040)
- Xu C, Xu XW, Dai FC, Saraf AK (2012b) Comparison of different models for susceptibility mapping of earthquake triggered landslides related with the 2008 Wenchuan earthquake in China. *Comput Geosci* 46:317–329. doi:[10.1016/j.cageo.2012.01.002](https://doi.org/10.1016/j.cageo.2012.01.002)
- Xu C, Xu XW, Yu GH (2013a) Landslides triggered by slipping-fault-generated earthquake on a plateau: an example of the 14 April 2010, Ms 7.1, Yushu, China earthquake. *Landslides* 10(4):421–431. doi:[10.1007/s10346-012-0340-x](https://doi.org/10.1007/s10346-012-0340-x)
- Xu C, Xu XW, Dai FC, Yao X (2013b) Three (nearly) complete inventories of landslides triggered by the May 12, 2008 Wenchuan Mw 7.9 earthquake of China and their spatial distribution statistical analysis. *Landslides*. doi:[10.1007/s10346-013-0404-6](https://doi.org/10.1007/s10346-013-0404-6)
- Xu C, Xu XW, Yao Q, Wang YY (2013c) GIS-based bivariate statistical modelling for earthquake-triggered landslides susceptibility mapping related to the 2008 Wenchuan earthquake, China. *Q J Eng Geol Hydrogeol* 46(2):221–236. doi:[10.1144/qjgeh2012-006](https://doi.org/10.1144/qjgeh2012-006)
- Xu C, Xu XW, Dai FC, Wu ZD, He HL, Wu XY, Xu SN, Shi F (2013d) Application of an incomplete landslide inventory, logistic regression model and its validation for landslide susceptibility mapping related to the May 12, 2008 Wenchuan earthquake of China. *Nat Hazards* 68(2):883–900. doi:[10.1007/s11069-013-0661-7](https://doi.org/10.1007/s11069-013-0661-7)
- Xu C, Xu XW, Zhou BG, Yu GH (2013e) Revisions of the M 8.0 Wenchuan earthquake seismic intensity map based on co-seismic landslide abundance. *Nat Hazards* 69(3):1459–1476. doi:[10.1007/s11069-013-0757-0](https://doi.org/10.1007/s11069-013-0757-0)
- Xu XW, Tan XB, Yu GH, Wu GD, Fang W, Chen JB, Song HP, Shen J (2013f) Normal- and oblique-slip of the 2008 Yutian earthquake: evidence for eastward block motion, northern Tibetan Plateau. *Tectonophysics* 584:152–165. doi:[10.1016/j.tecto.2012.08.007](https://doi.org/10.1016/j.tecto.2012.08.007)
- Yalcin A (2008) GIS-based landslide susceptibility mapping using analytical hierarchy process and bivariate statistics in Ardesen (Turkey): comparisons of results and confirmations. *Catena* 72(1):1–12. doi:[10.1016/j.catena.2007.01.003](https://doi.org/10.1016/j.catena.2007.01.003)
- Yamagishi H, Iwahashi J (2007) Comparison between the two triggered landslides in Mid-Niigata, Japan by July 13 heavy rainfall and October 23 intensive earthquakes in 2004. *Landslides* 4(4):389–397. doi:[10.1007/s10346-007-0093-0](https://doi.org/10.1007/s10346-007-0093-0)